

# Formation of stacking faults and their correlation with flux pinning and critical current density in Sm-doped $\text{YBa}_2\text{Cu}_3\text{O}_{7-\delta}$ films

Sung Hun Wee,<sup>1,\*</sup> Eliot D. Specht,<sup>1</sup> Claudia Cantoni,<sup>1</sup> Yuri L. Zuev,<sup>1,2</sup> Victor Maroni,<sup>3</sup> Winnie Wong-Ng,<sup>4</sup> Guangyao Liu,<sup>4</sup> Timothy J. Haugan,<sup>5</sup> and Amit Goyal<sup>1</sup>

<sup>1</sup>Materials Science and Technology Division, Oak Ridge National Laboratory, Oak Ridge, Tennessee 37831, USA

<sup>2</sup>Department of Physics, University of Tennessee, Knoxville, Tennessee 37996, USA

<sup>3</sup>Argonne National Laboratory, Argonne, IL 60439, USA

<sup>4</sup>Ceramic Division, National Institute of Science and Technology, Gaithersburg, MD 20899, USA

<sup>5</sup>AFRL/RZPG, The Air Force Research Laboratory, Wright-Patterson AFB, OH 45433, USA

(Received 15 April 2011; revised manuscript received 23 May 2011; published 29 June 2011)

A correlation between flux-pinning characteristics and stacking faults (SFs) formed by Sm substitution on Y and Ba sites was found in Sm-doped  $\text{YBa}_2\text{Cu}_3\text{O}_{7-\delta}$  films. It was confirmed that 223-type-SFs,  $\text{Y}_2\text{Ba}_2\text{Cu}_3\text{O}_x$ , composed of extra Y and O planes aligned parallel to the  $ab$ -planes formed via Sm substitution on the Y site and increased in number with increasing Sm doping on the Ba site. The number density of 223 SFs is correlated strongly with the enhancement in  $ab$ -plane-correlated flux pinning, resulting in a sharpening of the  $H\|ab$  peak in the plot of critical current density versus magnetic field orientation.

DOI: [10.1103/PhysRevB.83.224520](https://doi.org/10.1103/PhysRevB.83.224520)

PACS number(s): 74.72.-h, 74.25.Wx, 74.25.Sv, 74.78.Na

## I. INTRODUCTION

Flux-pinning and critical current density,  $J_c$ , for YBCO superconducting films has been remarkably strengthened by the controlled incorporation of nanoscale defects into the films.<sup>1-6</sup> In particular, epitaxial growth of self-organized, nonsuperconducting nanoscale defects aligned parallel to the  $c$ -axis of the film has resulted in strongly improved pinning and enhanced  $J_c$ , particularly for the case in which the magnetic field is also aligned parallel to the  $c$ -axis,  $H\|c$ .<sup>4-6</sup> In addition to the incorporation of nanoscale defects, rare-earth ( $R$ ) element substitution in YBCO has been considered a complementary method for synergistic enhancement of flux pinning. In fact,  $\text{R}\text{Ba}_2\text{Cu}_3\text{O}_{7-\delta}$  (RBCO) superconductors, especially those with  $R = \text{Nd}, \text{Sm}, \text{Eu},$  and  $\text{Gd}$  have been reported to result in superior superconducting performance, including larger  $T_c$ ,  $J_c$ , and irreversibility field,  $H_{\text{irr}}$ , as compared to undoped YBCO.<sup>7</sup> It has been argued that small amounts of  $R$  substitution into the Ba site (driven by their similar ionic sizes) create strong pinning centers that are nanoscale low  $T_c$  phases, without sacrificing the overall  $T_c$ .<sup>7</sup> Synergetic improvement in flux pinning by incorporation of  $\text{BaZrO}_3$  (BZO) into RBCO films has also been demonstrated.<sup>8,9</sup> However, fabrication of high-quality RBCO films requires modification of growth conditions with typically higher growth temperature and/or lower oxygen partial pressure or an additional seed layer to achieve 100%  $c$ -axis-oriented films and to suppress excess  $R$  substitution into the Ba site that significantly reduces  $T_c$ .<sup>10-12</sup> That is why the successful growth of high-quality RBCO films with higher self-field  $J_c$  compared to YBCO films is not commonly achieved.

Previous studies have demonstrated that partial  $R$  substitution onto the Y site would be a more effective and practical approach to achieving high  $J_c$  films without changing growth conditions.<sup>13-16</sup>  $\text{Y}_{1-x}\text{R}_x\text{BCO}$  films with  $R$  substitutions in the range of  $x = 0.1$  to  $0.5$  have been reported to have higher self-field  $J_c$  with enhanced in-field performance, as well as a higher  $T_c$  even though the samples were deposited at identical growth conditions to the YBCO films. Additional nanoscale

imperfections created by local strain fields associated with variations in ionic size between the  $R$  and  $Y$  have been considered as a possible origin for such  $J_c$  improvement.<sup>13-15</sup> However, there are no reports that clearly identify the types of defects that are dominantly formed and act as major pinning centers when the partial substitution of  $R$  elements is realized.

In this study, we discovered a particular type of defects that originated when Sm was substituted on the Ba site as well as on the Y site in YBCO films, and we investigated their correlation to flux-pinning characteristics.

## II. EXPERIMENTAL METHODS

$(\text{Y}_{0.667}\text{Sm}_{0.333+x})\text{Ba}_{2-x}\text{Cu}_3\text{O}_{7-\delta}$  (YSmBCO) films with different  $x$  in the range from 0 to 0.15 were grown by pulsed laser deposition (PLD). Selection of  $R$  element and the amount of  $R$  substitution for the parent ( $x = 0$ ) sample for this study was based on the previous study reporting that  $(\text{Y}_{0.667}\text{Sm}_{0.333})\text{Ba}_2\text{Cu}_3\text{O}_{7-\delta}$  had the highest  $J_c$  performance among  $\text{Y}_{1-x}\text{R}_x\text{BCO}$  samples with various  $R$  elements and substitution amounts.<sup>15</sup> PLD deposition conditions for the films were identical to those for pure YBCO films.<sup>6,17</sup> The film growth temperature,  $T_s$ , was 1063 K, and the oxygen partial pressure,  $P(\text{O}_2)$ , was 230 mTorr. All depositions were performed on ion-beam-assisted deposition (IBAD)-MgO templates with a  $\text{LaMnO}_3$  cap layer that were supplied by Superpower, Inc. A film thickness of  $\sim 800$  nm was confirmed by cross-sectional transmission electron microscopy (TEM) analysis. After deposition, the samples were *in situ* annealed at  $T_s = 773$  K and  $P(\text{O}_2) = 500$  Torr for 30 min. Ag electrodes were then sputtered onto the films followed by *ex situ* annealing at 773 K for 1 h in flowing  $\text{O}_2$  gas. In-field transport  $J_c$  of the samples was measured using the standard four-probe method while applying magnetic fields, after the samples were patterned to a  $200\text{-}\mu\text{m}$  bridge width by laser scribing. The angular dependence of  $J_c$  was measured in the maximum Lorentz force configuration in which the field direction is always perpendicular to the direction of the current. Cross-sectional microstructures were characterized by TEM. TEM

TABLE I. FWHM values of (006)  $\omega$ - and (113)  $\varphi$ -scans, % cube texture, transport  $T_c$ , and  $J_c$  at 77 K, self-field for 0.8- $\mu\text{m}$ -thick (Y,Sm)BCO films grown on IBAD-MgO templates.

Compositions of the samples	$\Delta\omega$ ( $^\circ$ )	$\Delta\varphi$ ( $^\circ$ )	% cube (%)	$T_c$ (K)	$J_c$ (77 K, sf) (MA/cm $^2$ )
YBa $_2$ Cu $_3$ O $_{7-\delta}$	1.3	3.2	96	87.7	2.8
(Y $_{0.667}$ Sm $_{0.333}$ )Ba $_{2.0}$ Cu $_3$ O $_{7-\delta}$	1.2	2.9	96	88.3	4.05
(Y $_{0.667}$ Sm $_{0.383}$ )Ba $_{1.95}$ Cu $_3$ O $_{7-\delta}$	1.1	2.8	95.5	88.4	3.05
(Y $_{0.667}$ Sm $_{0.433}$ )Ba $_{1.9}$ Cu $_3$ O $_{7-\delta}$	1.3	2.7	95.1	88.4	2.23
(Y $_{0.667}$ Sm $_{0.483}$ )Ba $_{1.85}$ Cu $_3$ O $_{7-\delta}$	1.3	2.7	96	87.4	0.82

cross-section specimens were prepared using the focused-ion beam (FIB) technique. Texture and phase analysis was performed using x-ray diffraction (XRD).

### III. EXPERIMENTAL RESULTS AND DISCUSSIONS

XRD results, including  $\theta$ - $2\theta$  scans, (006)  $\omega$ -scans, (113)  $\varphi$ -scans, and pole figures indicate that all the YSmBCO samples have excellent cube-on-cube epitaxy with 100%  $c$ -axis orientation. As summarized in Table I, the samples have small full-width-half-maximum (FWHM) values of in-plane ( $\Delta\varphi$ ) and out-of-plane ( $\Delta\omega$ ) orientations and sharp cube texture over 95%. However, as shown in Fig. 1(a), the YBCO (006) peak broadens with increasing amounts of Sm substitution. Bragg peak broadening is commonly analyzed using the Williamson-Hall plot,<sup>18</sup> where the scaled peak broadening is constant for finite-size and increases linearly with increasing

strain. As shown in Fig. 1(b), the broadening is oscillatory, indicating that stacking faults (SFs) are the cause. Hendricks and Teller describe in their Eq. (6) how one can calculate the diffraction pattern for a material consisting of randomly stacked layers of material.<sup>19</sup> In order to determine an unknown type of stacking fault, we simplify this formula by taking the limit where a fraction  $f \ll 1$  of the layers have thickness  $d_2$ , while the remaining fraction  $1-f$  has a thickness  $d_1$ . To first order in  $f$ , the Bragg reflection of order  $n$  has a Lorentzian line shape

$$I(2\theta) \sim [1 + 4(2\theta - 2\theta_0)^2/w^2]^{-2}, \quad (1)$$

where the peak FWHM is given by

$$w = 2f(1 - \cos \phi), \quad (2)$$

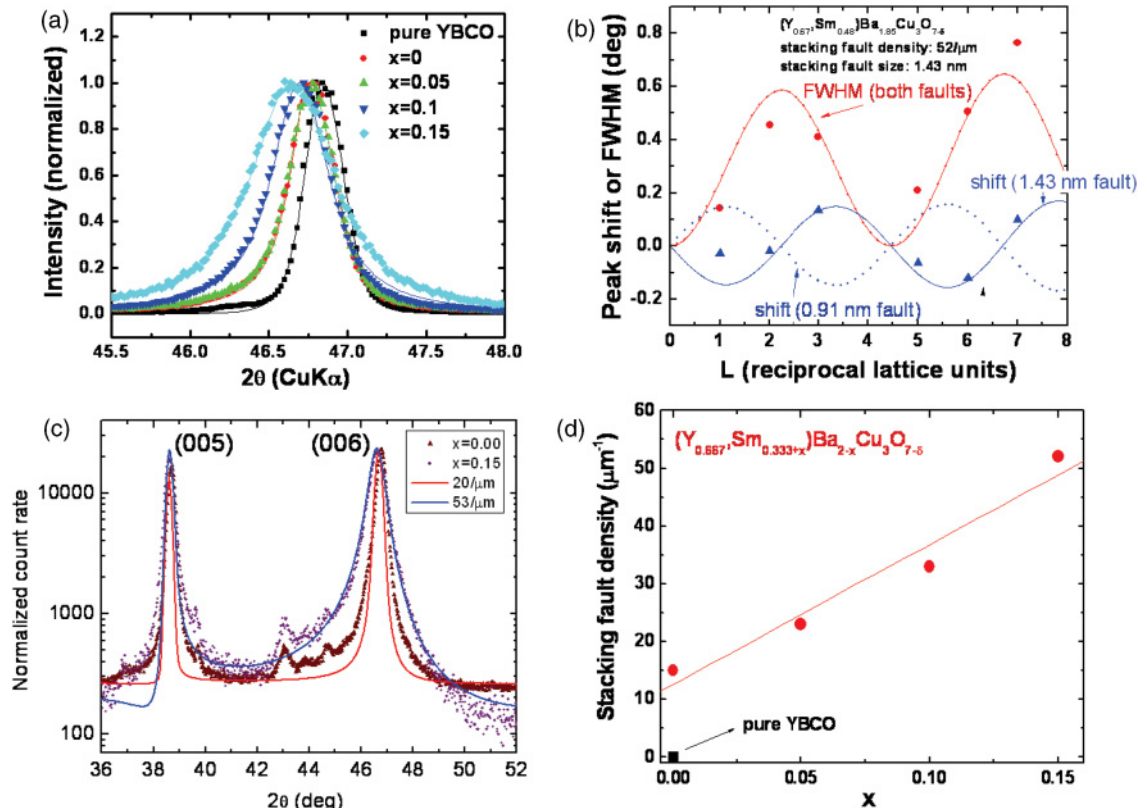


FIG. 1. (Color online) X-ray diffraction results for  $(Y_{0.667}Sm_{0.333+x})Ba_{2-x}Cu_3O_{7-\delta}$  films with  $x$  ranging from 0–0.15. (a)  $\theta$ - $2\theta$  scans showing broadening of the (006) peak with increasing  $x$ . (b) The width and shift of a series of (00 $l$ ) reflections. (c) Measured and simulated diffraction patterns for the  $x = 0$  and 0.15 samples. (d) SFs density estimated by Hendricks-Teller model as a function of  $x$ .

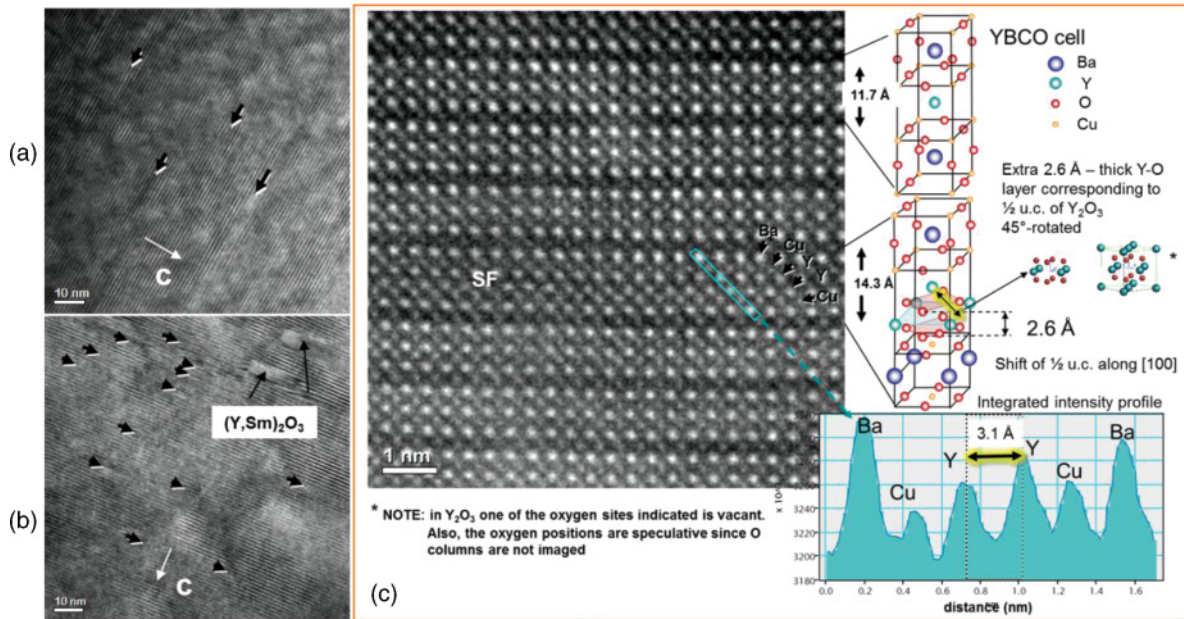


FIG. 2. (Color online) Cross-sectional TEM images for YSmBCO samples with (a)  $x=0$  and (b)  $x=0.15$ . (c) Z-contrast TEM image of a 223 SF, which includes extra Y and O layers (designed by arrow). Crystal structures representing YBCO and a 223 SF ( $Y_2Ba_2Cu_3O_x$ ) are illustrated in the right side of the figure. Note that in  $Y_2O_3$ , one of the oxygen sites indicated is vacant. Also, the oxygen positions in (c) are speculative since O columns are not distinguishable in the STEM image.

the peak shift is given by

$$2\theta_0 - 2\theta_1 = f\lambda\sin\phi/2\pi d_1\cos\phi, \quad (3)$$

where  $\phi = 4\pi d_2\sin\theta/\lambda$ , and  $\theta_1$  is the unshifted Bragg angle  $\theta_1 = \sin^{-1}(n\lambda/2d_1)$ . The nature of the stacking fault is determined by measuring the width and shift of a series of (00l) reflections and fitting the values to Eqs. (2) and (3) using  $f$  and  $d_2$  as free parameters. As shown in Fig. 1(b), a good fit to both the peak shifts and the peak widths is obtained for a stacking fault with a thickness of 1.43 nm. This corresponds well with the 223 stacking faults observed in YBCO having a thickness of 1.41 nm, consisting of extra planes of Y and O.<sup>20</sup> This is further confirmed by comparing the observed diffraction pattern to a simulated pattern using the complete Hendricks-Teller model, as shown in Fig. 1(c). Figure 1(d) shows the number density of 223 SFs as a function of the amount of Sm substitution estimated by the model. While no SFs for the pure YBCO sample are estimated, the SFs start forming in the case  $x=0$  when only Sm substitution into the Y site should occur and linearly increase with increasing Sm substitution on the Ba site up to a linear density of  $\sim 52 \mu\text{m}^{-1}$  at  $x=0.15$ .

Formation of 223 SFs was also visually confirmed by cross-sectional TEM examination of the same YSmBCO samples used for XRD analysis. Figures 2(a) and 2(b) show TEM images taken from the samples with Sm substitution on the Y site only ( $x=0$ ) and on both Y and Ba sites ( $x=0.15$ ). As denoted by black arrows, 223 SFs aligned along the  $ab$ -planes of the film are observed in both samples. The  $x=0.15$  sample has a higher number density of SFs than the  $x=0$  sample. This result is consistent with XRD measurements showing an increase in SF density with increasing  $x$ . Aberration-corrected Z-contrast (where  $Z$  = atomic number) scanning transmission

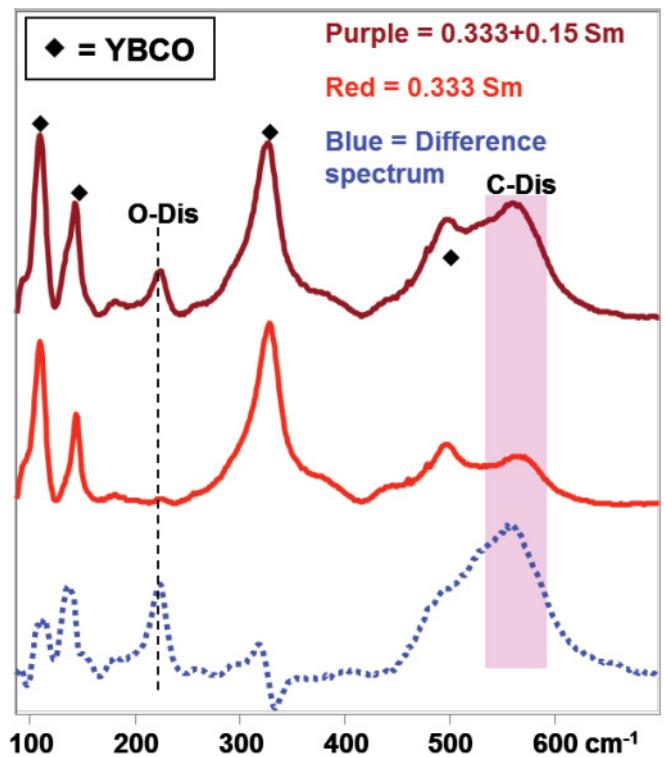


FIG. 3. (Color online) Raman spectra for YSmBCO films with  $x=0$  (red) and  $x=0.15$  (purple) with intensities normalized to the  $330 \text{ cm}^{-1}$  YBCO mode. These Raman spectra were excited using a 633-nm laser line. They comprise an averaged spectrum obtained by coadding spectra recorded at roughly 30 sample surface locations. The phonon modes at  $230 \text{ cm}^{-1}$  and  $560 \text{ cm}^{-1}$  indicate the presence of oxygen disorder and cation disorder, respectively (Ref. 21).



electron microscopy (STEM) imaging was also used to identify the atomic structure of 223 SFs as shown in Fig. 2(c), where the lattice image of a 223 SF having extra Y and O planes is shown. Crystal structures corresponding to YBCO and a 223 SF are illustrated in the right side of the figure.

Table I summarizes superconducting properties, including  $T_c$  and  $J_c$  at 77 K, self-field for the set of YSmBCO films with different  $x$  values. The data for a pure YBCO film prepared under an identical growth condition are also shown for comparison. All of the YSmBCO samples exhibit  $T_c$  of 87.4 ~ 88.3 K that are nearly unchanged from the  $T_c$  of 87.7 K for pure YBCO. However, there is considerable change in the  $J_c$  as a consequence of Sm substitution onto Y and Ba sites. First, the  $J_c$  is noticeably improved from 2.8 to 4.0 MA/cm<sup>2</sup> by Sm substitution on the Y sites. The  $J_c$  improvement can be ascribed to the formation of an optimal density of 223 SFs in the film. As reported from an earlier study of YBCO films with BZO additions, an optimum BZO doping also increases self-field  $J_c$  as well as in-field  $J_c$ .<sup>17</sup> However, after an initial enhancement,  $J_c$  gradually degrades with additional Sm substitution on the Ba sites. The  $J_c$  of the  $x = 0.05$  sample is reduced to ~3.4 MA/cm<sup>2</sup>, which is still larger than the  $J_c$  for pure YBCO.  $J_c$  drops further to 2.2 and 0.8 MA/cm<sup>2</sup>, with increasing  $x$  from 0.1 to 0.15.

There are two possible reasons for this reduction. First, the  $J_c$  can be reduced by the formation of second phases, such as Ba-Cu-O and CuO (or Cu<sub>2</sub>O), although no surface particles of these phases were observed. Excess Sm substitution on the Ba site can produce such excess phases, which can segregate at grain boundaries and reduce the  $J_c$ . Second, excess cation and oxygen disorder effects can develop with increasing Sm substitution on the Ba site and cause a reduction of  $J_c$ . In support of the latter cause for the observed  $J_c$  decrease, Raman spectroscopy measurements reveal a significant increase in phonon bands corresponding to both cation disorder and oxygen disorder with increasing Sm content, as shown in Fig. 3. This figure shows Raman spectra for YSmBCO films with  $x=0$  (red) and  $x=0.15$  (purple) with intensities normalized to the 330 cm<sup>-1</sup> YBCO mode, and the difference spectrum (blue dot line) obtained by subtracting the  $x=0$  spectrum from the  $x=0.15$  spectrum. The  $x=0.15$  sample has the much increased phonon modes at 230 cm<sup>-1</sup> and 560 cm<sup>-1</sup> that indicate significantly more cation disorder and oxygen disorder than the  $x=0$  sample. As shown in Fig. 4, an analysis of the intensity variations in a Z-contrast STEM image [similar to that shown in Fig. 2(c)] for the different cation columns also suggests that the cation disorder is localized within an area surrounding the 223 SF. This figure shows that far from

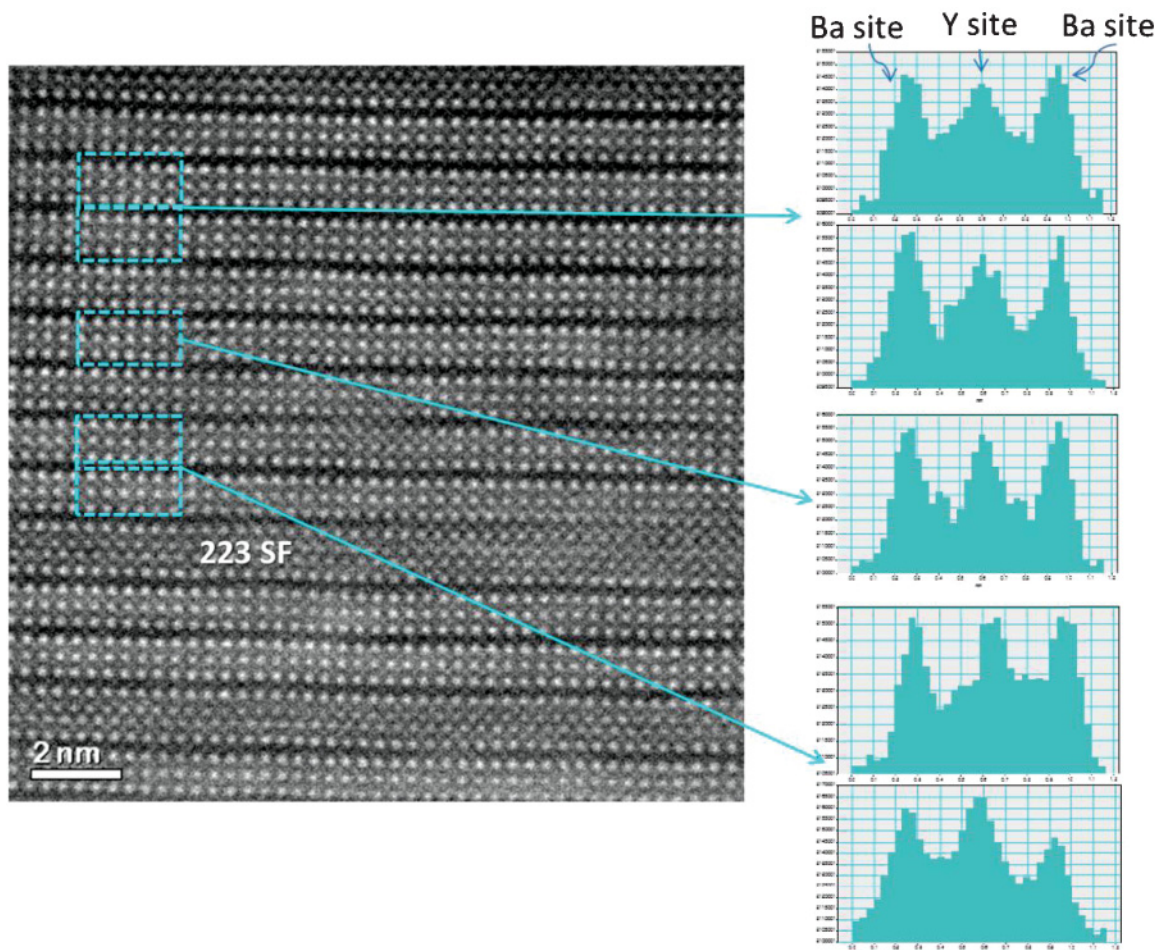


FIG. 4. (Color online) Aberration-corrected Z-contrast, cross-sectional STEM image for the  $x=0.15$  sample with integrated intensity profiles of atomic columns at the Y and Ba sites.

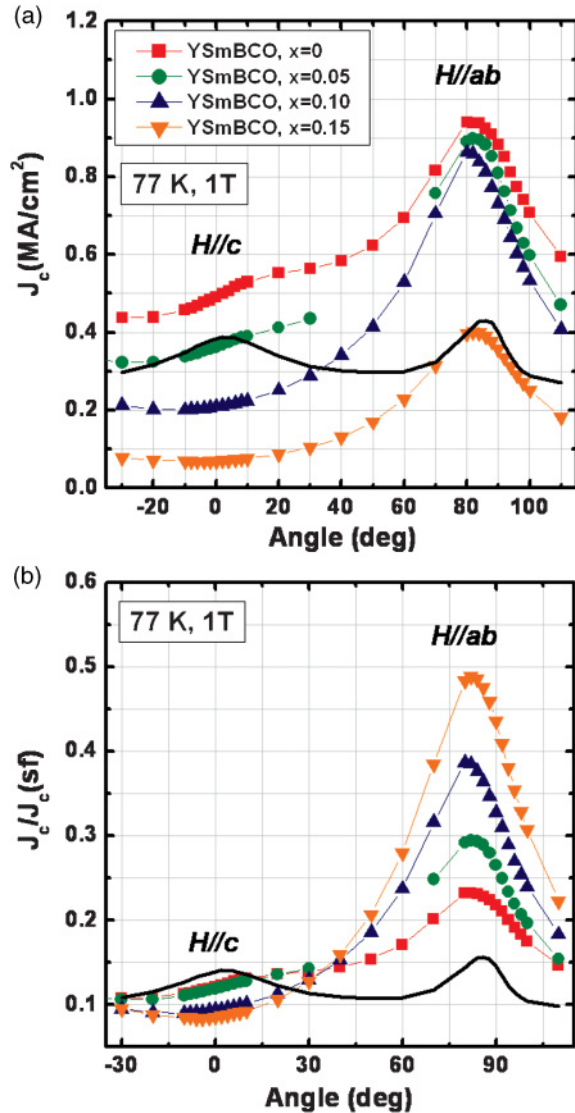


FIG. 5. (Color online) Angular dependence of  $J_c$  and  $J_c/J_c(sf)$  at 77 K and 1 T for pure YBCO and  $(Y_{0.667}Sm_{0.333+x})Ba_{2-x}Cu_3O_{7-\delta}$  films with  $x$  ranging from 0–0.15, in a magnetic field applied  $-30^\circ$  to  $110^\circ$  with respect to the  $c$ -axis of the film. For comparison,  $J_c$  data for the pure YBCO film with the same thickness are also plotted in the figure (black line).

the “223” SF, the collection of integrated intensity profiles has a higher intensity at the Ba site than at the Y site consistent with little or no cation disorder between the sites. However, the profile changes progressively with closer distance to the SF, where the intensity at the Y site becomes progressively higher than that at Ba sites, indicating the presence of significant cation disorder. Such localized nature of the cation disorder may explain the absence of  $T_c$  degradation for the samples with  $x$  values up to 0.15. In this situation a percolative path of zero resistance would exist during the low-current  $T_c$  measurement, while the self-field  $J_c$  would be significantly reduced given the degraded electronic properties of the disordered regions. Defect densities higher than those accommodating roughly all the vortices generated in the self-field can obviously be a reason for self-field  $J_c$  reduction, although they can further enhance in-field  $J_c$ . However, high  $J_c$  over 3 MA/cm<sup>2</sup> was

reported for solution processed YBCO films having a density of  $YBa_2Cu_4O_y$ , “124,” SFs of about  $68 \mu m^{-1}$ , which is higher than the SF density in the  $x=0.15$  sample ( $\sim 52 \mu m^{-1}$ ).<sup>22</sup>

The 223 SFs are expected to play the role of strong  $ab$ -plane-correlated pinning centers, resulting in an improvement of in-field  $J_c$ , particularly for a field parallel to the  $ab$ -plane,  $H//ab$ . The 124-type or  $Y_2Ba_4Cu_7O_y$ , 247-type SFs have been already demonstrated to act as strong  $ab$ -plane-correlated pinning centers to improve in-field  $J_c$  at  $H//ab$ . These SFs are also reported to be able to be random pinning centers when the field is away from  $H//ab$ .<sup>22–24</sup> Vortices could be pinned by the SFs themselves, or by the partial dislocations that form around the edges of a SF. Figure 5 presents the angular dependence of  $J_c$  and normalized  $J_c$  with respect to the self-field  $J_c$ ,  $J_c/J_c(sf)$  (sf), at 77 K, 1 T. As expected, much higher and sharper  $J_c$  peaks at  $H//ab$  are achieved for the samples with  $x$  values up to 0.1 due to the presence of 223 SFs in the films, compared to YBCO. For the  $x=0$  and 0.05 samples,  $J_c$  values for other field orientations away from  $H//ab$  are also larger than those for pure YBCO films due to their higher self-field  $J_c$  compared with pure YBCO. The  $x=0.15$  sample also shows a somewhat sharper  $J_c$  peak with a higher ratio of  $J_c(H//ab)/J_c(H//c)$ , but overall  $J_c$  values for the entire range of angles are much smaller due to the smaller self-field  $J_c$  of 0.8 MA/cm<sup>2</sup>, compared to the pure YBCO film. To investigate flux-pinning properties while excluding the effect caused by the difference in the self-field  $J_c$  between the samples, normalized  $J_c$  values for the samples are also compared in Fig. 5(b). It is obvious that Sm substitution remarkably enhances the flux pinning for  $H//ab$ . With increasing  $x$ , the peak of  $J_c/J_c(sf)$  for  $H//ab$  becomes sharper and significantly larger, while the  $J_c/J_c(sf)$  values near  $H//c$  are slightly reduced. Stronger  $ab$ -correlated pinning, resulting in sharper  $J_c/J_c(sf)$  peaks for  $H//ab$  with increasing  $x$ , is directly correlated to the increased number density of 223 SFs as confirmed by XRD and TEM analyses. Note that the increased cation and oxygen disorder with increasing values of  $x$  can also influence the flux pinning and in-field  $J_c$  properties of the samples. However, unlike the  $ab$ -plane-correlated pinning centers created by the 223 SFs, the disorder acts as isotropic-pinning centers and therefore influences flux pinning equally for all field angles. Such an isotropic pinning enhancement is not observed in these samples.

#### IV. CONCLUSION

In summary, the effect of Sm substitution on the Ba site as well as on the Y sites on the structural and superconducting properties of YSmBCO films has been investigated. Sm substitution on the Y and Ba sites in YBCO films gives rise to 223 SFs aligned along the  $ab$ -plane. The stacking fault density was found to increase with increasing amounts of Sm substitution. The sample designed to study only Sm substitution for Y ( $x=0$ ) resulted in the highest self-field  $J_c$  with strongly enhanced flux pinning for  $H//ab$ , which is probably due to forming an optimal density of the 223 SFs. As the value of  $x$  was increased from 0 to 0.15, corresponding to additional Sm substitution on the Ba-sites, the self-field  $J_c$  at 77 K gradually decreased. However, the flux pinning for  $H//ab$

was strongly enhanced by the increased number density of 223 SFs.

#### ACKNOWLEDGMENTS

We would like to thank SuperPower Inc. for providing the Hastelloy substrates with the multilayer configuration of IBAD MgO layer, homoepitaxial MgO layer, and epitaxial LaMnO<sub>3</sub>. This research was sponsored by the US Department of Energy (DOE) Office of Electricity Delivery and Energy Reliability – Advanced Cables and Conductors under Contract DE-AC05-

00OR22725 with UT-Battelle, LLC, managing contractor for Oak Ridge National Laboratory. Research also supported by ORNL's Shared Research Equipment (SHaRE) User Facility, which is sponsored by the Office of Basic Energy Sciences, US DOE. Use of Raman instrumentation at Argonne's Center for Nanoscale Materials was supported by the US DOE, Office of Science, Office of Basic Energy Sciences. The work performed at the Argonne National Laboratory was carried out under Contract DE-AC02-06CH11357 between UChicago Argonne, LLC, and the US DOE.

\*Corresponding author: wees@ornl.gov

<sup>1</sup>T. Haugen, P. N. Barnes, R. Wheeler, F. Meisenkothen, and M. Sumption, *Nature* **430**, 867 (2004).

<sup>2</sup>K. Matsumoto, T. Horide, A. Ichinose, S. Horii, Y. Yoshida, and M. Mukaida, *Jpn. J. Appl. Phys.* **44**, L246 (2005).

<sup>3</sup>J. L. Macmanus-Driscoll, S. R. Foltyn, Q. X. Jia, H. Wang, A. Serquis, L. Civale, B. Maiorov, M. E. Hawley, M. P. Maley, and D. E. Peterson, *Nat. Mater.* **3**, 439 (2004).

<sup>4</sup>A. Goyal, S. Kang, K. J. Leonard, P. M. Martin, A. A. Gapud, M. Varela, M. Paranthaman, A. O. Ijaduola, E. D. Specht, J. R. Thomson, D. K. Christen, S. J. Pennycook, and F. A. List, *Supercon. Sci. Technol.* **18**, 1533 (2005).

<sup>5</sup>S. H. Wee, A. Goyal, Y. L. Zuev, and C. Cantoni, *Supercon. Sci. Technol.* **21**, 092001 (2008).

<sup>6</sup>S. H. Wee, A. Goyal, E. D. Specht, C. Cantoni, Y. L. Zuev, V. Selvamanickam, and S. Cook, *Phys. Rev. B* **81**, 140503(R) (2010).

<sup>7</sup>M. Murakami, N. Sakai, T. Higuchi, and S. I. Yoo, *Supercon. Sci. Technol.* **9**, 1015 (1996).

<sup>8</sup>S. H. Wee, A. Goyal, P. M. Martin, M. Paranthaman, and L. Heatherly, *Supercon. Sci. Technol.* **19**, L42 (2006).

<sup>9</sup>T. Ozaki, Y. Yoshida, Y. Ichino, Y. Takai, K. Matsumoto, A. Ichinose, S. Horii, and M. Mukaida, *Physica C* **468**, 1615 (2008).

<sup>10</sup>C. Cantoni, D. P. Norton, D. M. Kroeger, M. Paranthaman, D. K. Christen, D. Verebelyi, R. Feenstra, D. F. Lee, and E. D. Specht, *Appl. Phys. Lett.* **74**, 96 (1999).

<sup>11</sup>Q. X. Jia, S. R. Foltyn, P. N. Arendt, H. Wang, J. L. MacManus-Driscoll, Y. Coulter, Y. Li, M. P. Maley, M. Hawley, K. Venkataraman and V. A. Maroni, *Appl. Phys. Lett.* **83**, 1388 (2003).

<sup>12</sup>S. H. Wee, A. Goyal, P. M. Martin and L. Heatherly, *Supercon. Sci. Technol.* **19**, 865 (2006).

<sup>13</sup>Z. S. Peng, J. M. Hao, B. Yin, Z. X. Zhao, Z. Q. Hua, and B. C. Yang, *Physica C* **282–287**, 2103 (1997).

<sup>14</sup>A. R. Devi, V. S. Bai, P. V. Patanjali, R. Pinto, N. H. Kumar, and S. K. Malik, *Supercon. Sci. Technol.* **13**, 935 (2000).

<sup>15</sup>J. L. MacManus-Driscoll, S. R. Foltyn, B. Maiorov, Q. X. Jia, H. Wang, A. Serquis, L. Civale, Y. Lin, M. E. Hawley, M. P. Maley, and D. E. Peterson, *Appl. Phys. Lett.* **86**, 032505 (2005).

<sup>16</sup>T. J. Haugan, T. A. Cambell, N. A. Pierce, M. F. Locke, I. Maartense, and P. N. Barnes, *Supercon. Sci. Technol.* **21**, 025014 (2008).

<sup>17</sup>A. Goyal, S. H. Wee, C. Cantoni, Y. L. Zuev, E. D. Specht, J. Shin, Y. Gao, S. Cook, O. Polat, T. Aytug, K. Kim, J. Sinclair, J. R. Thompson, M. P. Paranthaman, and D. K. Christen, presented at the 2009 Annual Peer Review for the US Superconductivity Program for Electric Systems, August 4–6, 2009, Washington, DC.

<sup>18</sup>B. D. Cullity and Stuart R. Stock, *Elements of X-ray Diffraction*, 3rd ed. (Prentice Hall, Upper Saddle River, NJ, 2001), p. 149.

<sup>19</sup>S. Hendrick and E. Teller, *J. Chem. Phys.* **10**, 147 (1942).

<sup>20</sup>C. L. Jia, H. Soltner, B. Kabius, U. Poppe, and K. Urban, *Physica C* **182**, 163 (1991).

<sup>21</sup>K. Venkataraman, R. Baurceanu, and V. A. Maroni, *Appl. Spectrosc.* **59**, 639 (2005).

<sup>22</sup>E. D. Specht, A. Goyal, P. M. Martin, X. Li, and M. Rupich, *Appl. Phys. Lett.* **89**, 162510 (2006).

<sup>23</sup>H. Yamasaki, K. Ohki, I. Yamaguchi, M. Sohma, W. Kondo, H. Matsui, T. Manabe, and T. Kumagai, *Supercon. Sci. Technol.* **23**, 105004 (2010).

<sup>24</sup>J. Wang, J. H. Kwon, J. Yoon, H. Wang, T. J. Haugan, F. J. Baca, N. A. Pierce, and P. N. Barnes, *Appl. Phys. Lett.* **92**, 082507 (2008).